



Disruption of protein kinase A localization induces acrosomal exocytosis in capacitated mouse sperm

Received for publication, February 6, 2018, and in revised form, April 19, 2018. Published, Papers in Press, April 26, 2018, DOI 10.1074/jbc.RA118.002286

Cintia Stival^{†1}, Carla Ritagliati^{†1}, Xinran Xu[§], Maria G. Gervasi[¶], Guillermina M. Luque^{||}, Carolina Baró Graf[‡], José Luis De la Vega-Beltrán^{**}, Nicolas Torres^{||}, Alberto Darszon^{**}, Diego Krapf^{§††}, Mariano G. Buffone^{||}, Pablo E. Visconti[¶], and Dario Krapf^{‡2}

From the [†]Laboratory of Cell Signal Transduction Networks, Instituto de Biología Molecular y Celular de Rosario (IBR), CONICET-UNR, Rosario 2000, Argentina, the [§]Department of Electrical and Computer Engineering, Colorado State University, Fort Collins, Colorado 80523, the [¶]Department of Veterinary and Animal Sciences, University of Massachusetts, Amherst, Massachusetts 01003, the ^{||}Instituto de Biología y Medicina Experimental (IBYME), Consejo Nacional de Investigaciones Científicas y Tecnológicas (CONICET), Buenos Aires C1428ADN, Argentina, the ^{**}Departamento de Genética del Desarrollo y Fisiología Molecular, Instituto de Biotecnología (IBT), Universidad Nacional Autónoma de México (UNAM), Cuernavaca, Morelos 62210, México, and the ^{‡††}School of Biomedical Engineering, Colorado State University, Fort Collins, Colorado 80523

Edited by Alex Toker

Protein kinase A (PKA) is a broad-spectrum Ser/Thr kinase involved in the regulation of several cellular activities. Thus, its precise activation relies on being localized at specific subcellular places known as discrete PKA signalosomes. A-Kinase anchoring proteins (AKAPs) form scaffolding assemblies that play a pivotal role in PKA regulation by restricting its activity to specific microdomains. Because one of the first signaling events observed during mammalian sperm capacitation is PKA activation, understanding how PKA activity is restricted in space and time is crucial to decipher the critical steps of sperm capacitation. Here, we demonstrate that the anchoring of PKA to AKAP is not only necessary but also actively regulated during sperm capacitation. However, we find that once capacitated, the release of PKA from AKAP promotes a sudden Ca²⁺ influx through the sperm-specific Ca²⁺ channel CatSper, starting a tail-to-head Ca²⁺ propagation that triggers the acrosome reaction. Three-dimensional super-resolution imaging confirmed a redistribution of PKA within the flagellar structure throughout the capacitation process, which depends on anchoring to AKAP. These results represent a new signaling event that involves CatSper Ca²⁺ channels in the acrosome reaction, sensitive to PKA stimulation upon release from AKAP.

Mammalian sperm require two post-testicular maturation steps to become fertile: epididymal maturation, occurring in the male epididymis, and capacitation, occurring after ejaculation in the female tract. This process is associated with changes in the sperm motility pattern known as hyperactivation, and with the preparation to undergo the acrosome reaction, an exocytotic process, upon exposure to physiological agonists (1). Capacitation is a highly complex process orchestrated by protein kinase A (PKA)³ activity (2). Its activation appears to be necessary for: 1) membrane potential (*Em*) hyperpolarization (3, 4), which originates after 15–30 min; 2) development of hyperactivated motility after 30–45 min; and 3) triggering of the acrosome reaction, once capacitation is complete, *i.e.* after 60 min for mouse sperm. Even though these processes differ in their kinetics, all of them involve phosphorylation cascades initiated by PKA. Moreover, one of the first signaling pathways observed during capacitation is the HCO₃⁻-dependent stimulation of cAMP synthesis, which rapidly activates PKA (5).

Being PKA, a promiscuous Ser/Thr kinase, its precise activation at specific localizations, known as discrete PKA signalosomes, is necessary (6). However, PKA localization can vary over time, and these changes have been proposed to regulate different processes (7, 8). PKA associates to cellular structures through A-Kinase anchoring proteins (AKAPs), which form scaffolding assemblies that play a pivotal role in PKA regulation. AKAPs restrict PKA activity to specific microdomains dependent on the regulation of PKA–AKAP interaction. Most AKAPs also anchor other signaling enzymes such as cyclic nucleotide phosphodiesterases that degrade cAMP and allow PKA activation to be locally regulated in amplitude and duration. Synthetic peptides bearing an amphipathic helix domain that interacts with the PKA regulatory II subunits (PKARII), also

This work was supported by Agencia Nacional de Promoción Científica y Tecnológica Grants PICT 2014-2702 and PICT 2015-3164 (to Dario Krapf) and PICT 2015-2294 (to M. G. B.), Dirección General de Asuntos del Personal Académico/Universidad Nacional Autónoma de México Grant IN205516 and Consejo Nacional de Ciencia y Tecnología Fronteras 71 (to A. D.), National Science Foundation Grant 1401432 (to Diego Krapf), Eunice Kennedy Shriver National Institutes of Health, NICHD Grants RO1 HD38082 and HD44044 (to P. E. V.), and National Institutes of Health Grant RO1TW008662 (to M. G. B.). The authors declare that they have no conflicts of interest with the contents of this article. The content is solely the responsibility of the authors and does not necessarily represent the official views of the National Institutes of Health.

This article contains Movies S1–S6.

¹ Both authors contributed equally to this work.

² To whom correspondence should be addressed: Instituto de Biología Molecular y Celular de Rosario (CONICET-UNR) and Laboratorio de Especialidades Reproductivas, Facultad de Ciencias Bioquímicas y Farmacéuticas, UNR, Ocampo y Esmeralda, Rosario 2000, SF, Argentina. Tel.: 54-341-423-7070 (ext. 654); E-mail: krapf@ibr-conicet.gov.ar.

³ The abbreviations used are: PKA, protein kinase A; Bt₂AMP, dibutylryl cyclic AMP; 8Br-cAMP, 8Br-cAMP; IBMX, isobutylmethylxanthine; 3D STORM, three-dimensional stochastic optical reconstruction microscopy; AKAP, A-Kinase anchoring protein; PKAR, PKA regulatory; CASA, computer-assisted semen analysis; ROI, regions of interest; CAP, capacitating; NC, non-capacitating; GLUT3, glucose transporter 3; *Em*, membrane potential; EGFP, enhanced green fluorescent protein.

This is an Open Access article under the CC BY license.



PKA relocation in sperm capacitation and acrosome reaction

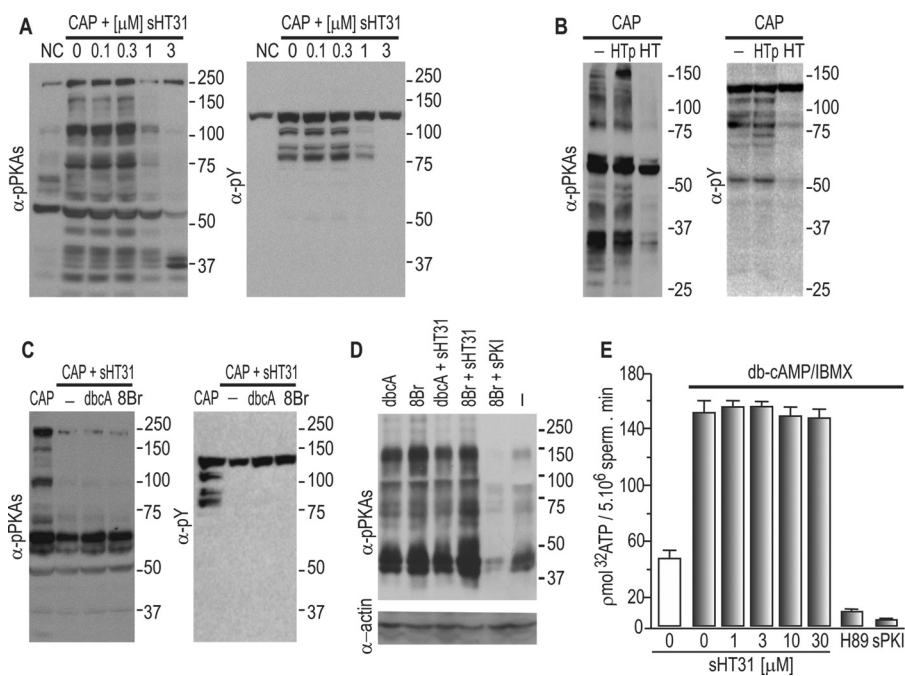


Figure 1. Inhibition of PKA–AKAP interaction abrogates phosphorylation cascades associated with sperm capacitation. A–C, Western blot analysis with α -pPKAs (left panel) and α -pY antibodies (right panel) of protein extracts obtained from the following conditions: A, mouse sperm incubated in the absence or presence of increasing sHT31 concentrations for 60 min in capacitating (CAP) or noncapacitating (NC) media. B, sperm were incubated in capacitating medium (CAP) in the absence or presence of either 3 μM sHT31 (HT) or 6 μM sHT31p (HTp, the inactive sHT31 analogue) as a specificity control. C, sperm incubated for 60 min in CAP containing 1 μM sHT31 in the presence or absence of 1 mM Bt₂cAMP, 0.1 mM IBMX (dbcA), or 1 mM 8Br-cAMP, 0.1 mM IBMX (8Br). D, analysis of PKA activity in cell-free assays. Sperm were incubated for 30 min in medium containing 40 μM ATP, 1 mM Bt₂cAMP (dbcA), or 1 mM 8Br-cAMP (8Br), 0.1 mM IBMX, 10 mM MgCl₂, and 1% Triton X-100, in the absence or presence of 3 μM sHT31 or 15 μM sPKI. Negative control lane (–) does not contain Bt₂cAMP. Each condition was processed for Western blot analysis and immunodetected with α -pPKAs antibody and α -actin, which was used as a loading control. E, sperm PKA activity was measured as described under “Experimental procedures” using Kempptide as PKA substrate. Kinase buffer contained the indicated amounts of sHT31, 30 μM H89, or 15 μM sPKI, maintaining a constant concentration of DMSO. Negative control lane (white bar) does not contain Bt₂cAMP. Data represent mean \pm S.E. of three independent experiments performed in triplicates.

known as PRKAR2) impair PKA binding to AKAPs (9). These peptides, commonly used as tools to disrupt subcellular PKA localization, contain an N-terminal modification with a stearic acid moiety that confers membrane permeability. One example of this type of amphipathic peptide is sHT31, a 24-residue peptide that binds to PKARII with high affinity (9) preventing their interaction with AKAPs.

In this article, we used the peptide sHT31 to investigate how disruption of PKA–AKAP interaction affects sperm parameters associated to fertilizing capacity. We observed that the release of PKA from AKAP in capacitated sperm promotes a sudden influx of Ca²⁺ that starts in the principal piece, and propagates to the head triggering the acrosome reaction. This process was not observed in cells lacking the sperm-specific voltage-dependent Ca²⁺ channel complex CatSper. In addition, we used three-dimensional stochastic optical reconstruction microscopy (3D STORM) to study spatial distribution of PKA catalytic subunit α 2 (cPKA, also known as PRKACA2) in mouse sperm, which provides 3D information with resolution of \sim 20 nm (10, 11). We observed that upon capacitation, the catalytic subunit redistributes within the flagellum. This movement was completely abrogated when sperm were exposed to sHT31. Altogether, these data indicate that PKA localization and anchoring to AKAPs are actively regulated during sperm capacitation. In addition, our findings show that once the sperm is capacitated, delocalization of the catalytic subunit alters PKA-dependent signaling pathways, elevates

intracellular Ca²⁺, and, in turn, induces the acrosome reaction. This work provides evidence for the involvement of flagellar CatSper channels in the acrosome reaction that takes place in the head.

Results

sHT31 disrupts sperm capacitation–associated pathways

The exposure of cells to PKA-anchoring disruptor peptides has been shown to promote an ablation of compartmentalized PKA signaling (12). To study the role of PKA anchoring in the sperm capacitation–associated pathways, we used the peptide sHT31, which inhibits the interaction between PKARII and AKAP (9). sHT31 is the permeable steared form of a short peptide composed of 24 residues (N-stearate-DLIEEAASRIV-DAVIEQVKAAGAY) from the PKA-anchoring domain of AKAP. To disrupt PKA–AKAP interaction, sperm were preincubated for 10 min with different sHT31 concentrations before exposure to conditions that support capacitation. Western blot analysis shows that this preincubation with sHT31 blocked the phosphorylation of PKA substrates associated with sperm capacitation (13), with an IC₅₀ below 1 μM (Fig. 1A left panel). These data indicates that PKA anchoring is crucial for proper PKA activity. Tyrosine phosphorylation, which occurs downstream of PKA activation (2), was also blocked (Fig. 1A, right panel). As a negative control, a second peptide was used (sHT31p), in which two isoleucine residues are replaced by pro-

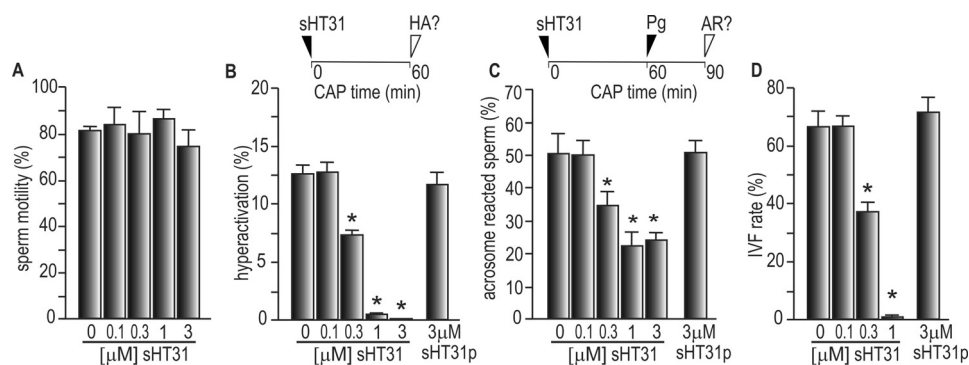


Figure 2. PKA anchoring inhibition impairs sperm capacitation. A and B, mouse sperm were incubated in the absence or presence of different sHT31 concentrations or sHT31p for 60 min in medium that supports capacitation. Sperm motility was examined using the CEROS CASA system. Total (A) and hyperactivated (B) motility are indicated. Data represent mean \pm S.E., $n = 3$; $p < 0.01$. C, sperm were capacitated (CAP) for 60 min in media containing the specified concentrations of sHT31 or sHT31p before incubation with 40 μ M progesterone (Pg) for 30 min. Acrosomal status (AR) was assessed by fluorescence microscopy. Data represent mean \pm S.E., $n \geq 3$, $p < 0.01$. D, sperm were capacitated in either the presence or absence of sHT31 or sHT31p. After capacitation, eggs were inseminated with 2.5×10^6 sperm/ml in 200- μ l drops. *In vitro* fertilization (IVF) was assessed by microscopic visualization of pronuclei formation. Data represent mean \pm S.E., $n = 3$; $p < 0.01$. At least 30 eggs were evaluated for each treatment.

line residues, rendering this peptide unable to disrupt the PKARII–AKAP interaction (9). This control peptide did not block PKA activity even when used at twice the maximum concentration of sHT31 (6 μ M) (Fig. 1B).

The effect of sHT31 on capacitation-induced phosphorylation pathways in live sperm suggests that disruption of PKA–AKAP anchoring inhibits the ability of this kinase to find its physiological substrates. However, these results could also be explained by a direct effect on cAMP synthesis or PKA catalytic activity. To evaluate the extent by which the sHT31 effect was due to reduced levels of cAMP, sperm incubated with sHT31 were also treated with the cAMP permeable agonists Bt₂cAMP or 8Br-cAMP in the presence of the broad-spectrum inhibitor of cyclic nucleotide phosphodiesterases IBMX. In these conditions, the sHT31 peptide still blocked phosphorylation of PKA substrates (Fig. 1C, left panel) and the increase in tyrosine phosphorylation (Fig. 1C, right panel) indicating that the sHT31 target is downstream of cAMP synthesis. To evaluate whether sHT31 has a direct effect on PKA catalytic activity, we used two different approaches. First, we prepared whole cell-free sperm extracts by incubating sperm in 1% Triton X-100 buffer (see “Experimental procedures”). These extracts were treated with Bt₂cAMP and IBMX in the presence of either 3 μ M sHT31 or 15 μ M sPKI (a permeable pseudo-substrate of PKA that specifically inhibits PKA). Western blots revealed that Bt₂cAMP induced phosphorylation of PKA substrates in cell-free extracts, which was blocked with sPKI, but not with sHT31 (Fig. 1D). Moreover, when PKA activity was measured using radioactive ATP and Kemptide as a substrate (13), sHT31 did not produce an inhibitory effect, even at 30 μ M (Fig. 1E), whereas two well-established PKA inhibitors (H89 and sPKI) blocked Kemptide phosphorylation, as expected. These data ruled out sHT31 off-target effects on cAMP synthesis and PKA activity.

Disruption of PKA localization blocks sperm functional parameters

The main functional events of sperm acquisition of fertilizing capacity are hyperactivated motility and the preparation for the acrosome reaction. The cAMP/PKA pathway in sperm is one of the initial events of capacitation. To evaluate the effect of dis-

rupting the PKA–AKAP interaction on the acquisition of fertilizing capacity, sperm were incubated in the presence of increasing sHT31 concentrations. We observed that whereas sperm motility was not affected by sHT31 concentrations below 3 μ M (Fig. 2A), sperm treated with sHT31 were unable to hyperactivate (Fig. 2B), undergo the acrosome reaction (Fig. 2C), and fertilize *in vitro* (Fig. 2D).

Inhibition of PKA–AKAP interaction in capacitated sperm promotes the acrosome reaction

Capacitation-induced hyperpolarization of the plasma *Em* has been shown to be essential to prepare sperm for the acrosome reaction (16). In addition, *Em* hyperpolarization was reported to be dependent on PKA activity (3). Thus, considering the diminished acrosome reaction obtained (Fig. 2C), we addressed the effect of PKA–AKAP inhibition on *Em* hyperpolarization, using the carbocyanine dye DISC₃(5) in a fluorimetric population assay (5). Fig. 3A shows that disruption of the PKA–AKAP interaction with sHT31 effectively blocked the capacitation-induced *Em* hyperpolarization at 1 μ M. Taking all these results into consideration, we analyzed whether PKA–AKAP interaction is still necessary for the acrosome reaction once *Em* hyperpolarization is achieved. To this aim, sperm were allowed to capacitate for 60 min, then exposed to 1 μ M sHT31, and *Em* was measured at 70, 80, and 90 min. To our surprise, a time-dependent *Em* depolarization was observed (Fig. 3, B and C). This depolarization correlated to the triggering of the acrosome reaction by sHT31, as seen by cytometric analysis using transgenic mice expressing EGFP in their acrosomal vesicles (Fig. 4, A–C) or by acrosomal staining of WT mice (Fig. 4D). However, the acrosome reaction was only induced by sHT31 (at concentrations 1 and 3 μ M) in capacitated sperm, but not in noncapacitated sperm, nor when capacitated sperm were exposed to the inactive analogue sHT31p (Fig. 4, C and D). This result points toward the need of active PKA for the induction of the acrosome reaction, indicating that a sudden delocalization of active PKA in capacitated sperm triggers the acrosome reaction. Accordingly, when capacitated sperm were exposed to either 30 μ M KT5720 or 15 μ M sPKI, two mechanistically different PKA inhibitors, sHT31 failed to induce the acrosome

PKA relocation in sperm capacitation and acrosome reaction

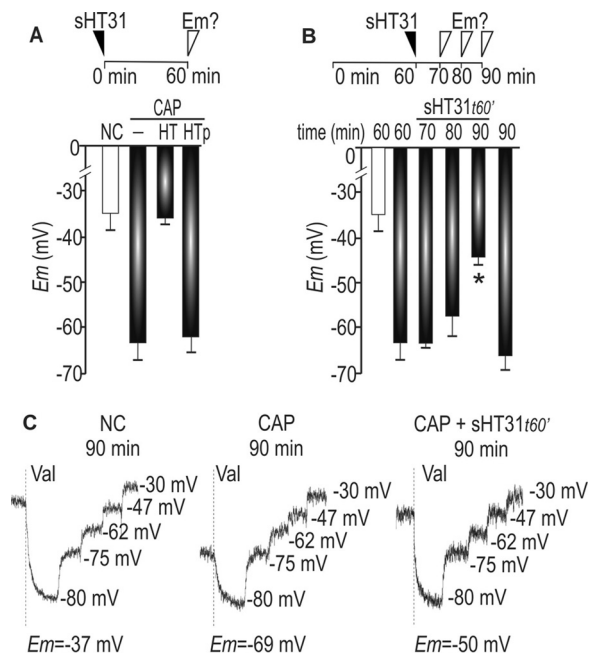


Figure 3. Effect of PKA–AKAP disruption on E_m . A, E_m measurements of sperm incubated for 60 min in noncapacitating (NC, white bar) or capacitating (CAP, gray bars) conditions containing $1 \mu\text{M}$ sHT31 (HT) or sHT31p (HTp), using DISC₃(5) in a population assay. Data represent mean \pm S.E., $n \geq 3$, $p < 0.01$. B, E_m recordings were obtained after 60 min of incubation in noncapacitating (white bar) or capacitating (gray bars) conditions. Alternatively, $1 \mu\text{M}$ sHT31 was added at 60 min, and E_m analyzed after 10, 20, or 30 min, as indicated. Data represent mean \pm S.E., $n \geq 3$, $p < 0.01$. C, fluorescence traces showing the values of E_m obtained after sperm incubation for 90 min in noncapacitating, capacitating, or capacitating media exposed to $1 \mu\text{M}$ sHT31 at time 60 min (CAP + sHT31t60'). Each experiment displays its calibration curve.

reaction (Fig. 4E). These data indicate that when PKA anchoring is blocked in capacitated sperm, PKA activity promotes the acrosome reaction.

Acrosome reaction triggered by inhibition of PKA–AKAP interaction in capacitated sperm correlates with Ca^{2+} influx through CatSper channels

Pharmacologically hyperpolarized noncapacitated sperm undergo the acrosome reaction when depolarized (e.g. addition of high K^+ concentrations), or exposed to solubilized zona pelliculadae (16). In view of these findings, we questioned the relationship between E_m depolarization triggered by sHT31 (Fig. 3B) and the onset of acrosome reaction (Fig. 4C). Two hypotheses arose: 1) depolarization triggers the acrosome reaction; and 2) depolarization is the consequence of a Ca^{2+} influx, which triggers the acrosome reaction. To test the first hypothesis, noncapacitated sperm were pharmacologically hyperpolarized with valinomycin before being exposed to sHT31. As seen in Fig. 5A, sHT31 was not capable of inducing the acrosome reaction on hyperpolarized noncapacitated sperm. Furthermore, when sperm were capacitated in medium with valinomycin and 70 mM extracellular K^+ , abrogating sperm E_m hyperpolarization (16), sHT31 was still able to trigger the acrosome reaction (Fig. 5A). In a control experiment, capacitated sperm clamped at depolarized E_m lost the ability to undergo the acrosome reaction when challenged with progesterone (Fig. 5A). These results imply that E_m hyperpolarization is neither necessary nor sufficient for sHT31 to induce the acrosome

reaction, and argues against the first hypothesis. To test the second hypothesis, we exposed capacitated sperm to the Ca^{2+} channel blocker mibefradil before adding sHT31. This procedure blocked the depolarization (Fig. 5B) and the acrosome reaction (Fig. 5C) induced by sHT31, supporting the second hypothesis. Moreover, when 3.5 mM EGTA (free Ca^{2+} of 138 nM as measured with MaxChelator software (17)) was added before sHT31, the acrosome reaction was also blocked (Fig. 5C), further substantiating the role of Ca^{2+} influx as the cause of depolarization and acrosome reaction.

We performed intracellular Ca^{2+} concentration ($[\text{Ca}^{2+}]_i$) measurements of Fluo3-AM–loaded spermatozoa on laminin-coated coverslips, to allow analysis of live sperm where the flagellum remains free and moving. Fig. 6 shows that $[\text{Ca}^{2+}]_i$ increased upon disruption of PKA–AKAP interaction, only in capacitated sperm (Fig. 6 and Movie S1). As expected, this $[\text{Ca}^{2+}]_i$ increase was absent in noncapacitated sperm (Fig. 6 and Movie S2) and in capacitated sperm exposed to the inactive analogue sHT31p (Fig. 6 and Movie S3). Moreover, $5 \mu\text{M}$ mibefradil affected the amplitude of the signal, further supporting the hypothesis that a Ca^{2+} channel (either T-type or CatSper) is involved in the Ca^{2+} entry (Fig. 6 and Movie S4). In agreement with the inhibition of acrosome reaction by PKA inhibitors, when sperm were preincubated with sPKI for 10 min before exposure to sHT31, the $[\text{Ca}^{2+}]_i$ increase caused by PKA–AKAP disruption was absent (Fig. 6 and Movie S5).

To analyze $[\text{Ca}^{2+}]_i$ in the different cellular domains we performed measurements of $[\text{Ca}^{2+}]_i$ using concanavalin A-coated coverslips (attaching the whole cell to the coverslip) and increased frame rates (10 Hz, 100 ms/frame). The $[\text{Ca}^{2+}]_i$ increase was first evidenced at the principal piece, followed by an increase in the mid-piece and later propagation to the head, as shown by a representative Ca^{2+} kymograph in Fig. 7A and Movie S6. The mean of Ca^{2+} fluctuation in the different subregions is shown in Fig. 7B, indicating the delays of Ca^{2+} signal propagation. Considering that CatSper channel locates to the principal piece (18), and is blocked by low mibefradil concentrations, these results substantiate the role of CatSper in sHT31-promoted Ca^{2+} influx. Accordingly, CatSper is the only Ca^{2+} channel in sperm that is supported by solid electrophysiological evidence and the Ca^{2+} channel-blocker mibefradil has been shown to inhibit CatSper currents (19). As shown by previous works, when extracellular medium is deprived of Ca^{2+} and Mg^{2+} , CatSper becomes permeable to Na^+ , which can be clearly evidenced by the Na^+ -dependent depolarization upon Ca^{2+} chelation (20, 21). The magnitude of this depolarization depends on the extent of CatSper opening. Therefore, by studying sperm E_m in population assays using the fluorophore DISC₃(5), we addressed whether PKA–AKAP disruption triggers CatSper opening after EGTA addition. When capacitated sperm loaded with DISC₃(5) were first exposed to EGTA and then to $1 \mu\text{M}$ sHT31, CatSper opening was evidenced by E_m depolarization (Fig. 7, C and D). When $0.1 \mu\text{M}$ sHT31 was used, depolarization was observed to a lesser extent, whereas no depolarization was detected when noncapacitated sperm were exposed to $1 \mu\text{M}$ sHT31, consistent with the requirement of active PKA upon inhibition of AKAP anchoring. To further demonstrate the role of CatSper in the Ca^{2+} influx conductive

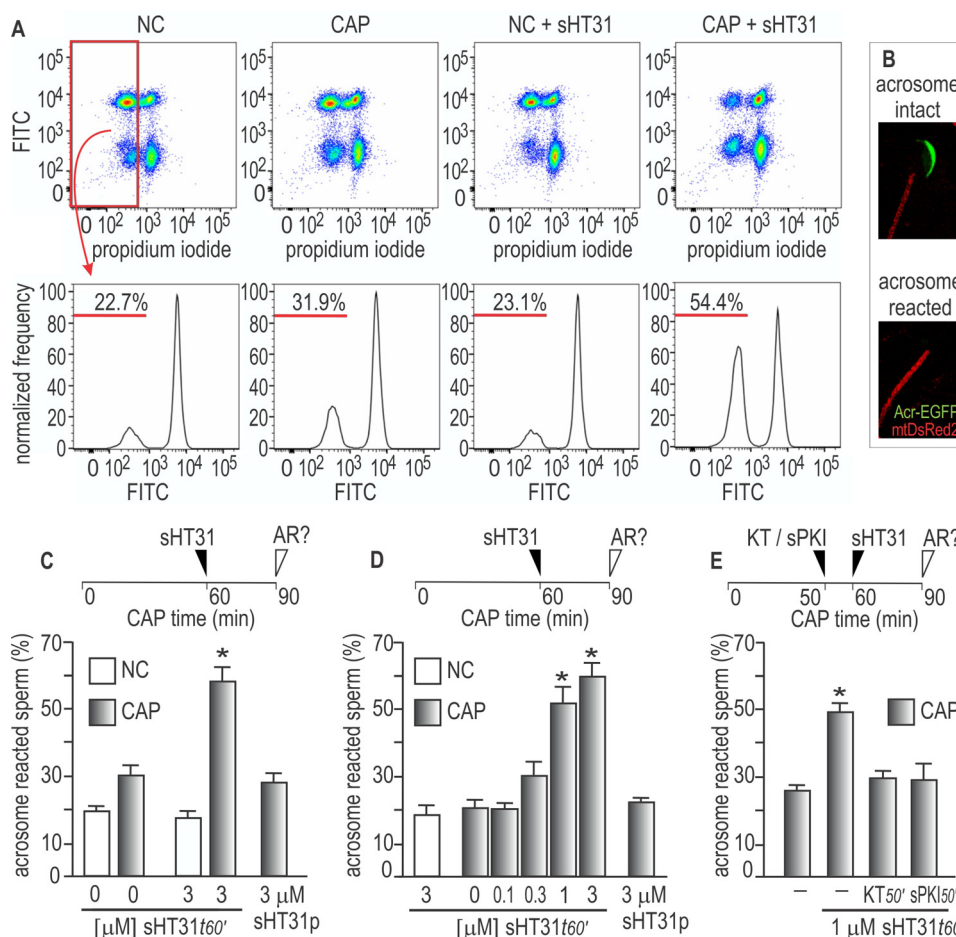


Figure 4. Acrosome reaction is modulated by PKA anchoring. A–C, sperm were incubated in capacitating (CAP) or noncapacitating conditions (NC) during 60 min before addition of sHT31 and further incubation for 30 min. Acrosomal status was assessed by flow cytometry using sperm expressing EGFP under the acrosin promoter (*Acr-EGFP*). A, FITC versus propidium iodide two-dimensional fluorescence dot plot analysis. These two-dimensional dot plots were used to distinguish between sperm with low (live) and high (dead) propidium iodide staining. Histogram analysis depicting normalized frequency of sperm and FITC fluorescence were performed in live sperm populations, with the corresponding percentage of acrosome-reacted sperm (with low FITC fluorescence). Representative images of four independent experiments are shown. B, representative confocal images showing transgenic acrosome-intact and acrosome-reacted sperm. These transgenic mice have acrosomal vesicles expressing green EGFP fluorescence and mid-pieces (mitochondria) expressing red Ds-Red2 fluorescence. C, percentage of sperm that decreased FITC fluorescence (acrosome reacted, AR). Data represent mean \pm S.E. of at least five independent experiments, *, $p < 0.01$. D, sperm were incubated in noncapacitating (NC, white bar) or capacitating conditions (gray bars) during 60 min followed by addition of the specified concentrations of sHT31 or sHT31p and further incubation for 30 min, before assessment of acrosomal status (AR) by acrosomal staining. E, sperm were incubated in capacitating conditions during 50 min followed by addition of either 15 μ M sPKI or 30 μ M KT5720 (KT), two different PKA inhibitors, for 10 min time after which 1 μ M sHT31 was added and further incubated for 30 min. Data represent mean \pm S.E. of at least three independent experiments, *, $p < 0.01$.

to the acrosome reaction, CatSper KO mice were used. sHT31 failed to trigger acrosome reaction in CatSper KO (Fig. 7E). As a control, WT siblings (-/+) underwent normal acrosome reaction induced by sHT31. It is worth noticing that the Ca^{2+} ionophore A23187 promoted normal acrosome reaction both in WT and CatSper KO sperm.

PKA localization changes revealed by super-resolution imaging

To analyze PKA localization dynamics during capacitation, 3D STORM was used, enabling the study of spatial distribution of PKA catalytic subunit $\alpha 2$ (cPKA, also known as PRKACA2) in mouse sperm. This type of microscopy allows 3D reconstruction with resolution of ~ 20 nm (10, 11), to study protein distribution within the narrow sperm tail, which is less than 1 μ m in diameter. The spatial distribution of cPKA was determined in both noncapacitated and capacitated sperm. As shown in Fig. 8A, noncapacitated sperm exhibited a dense and

compact rod-like radial distribution of cPKA. The facilitative glucose transporter 3 (GLUT3), which is present throughout the flagellar plasma membrane (22), showed a continuous ring staining cross-section. This was used as a control, showing a distribution compatible with previous reports (23) (Fig. 8, A and B) and validating the structural information obtained by 3D STORM.

Interestingly, upon capacitation, cPKA localized to a broader cylinder-like distribution. Fig. 8B shows the radial localization of cPKA in capacitated and noncapacitated sperm as well as the distribution of GLUT3. The distribution of cPKA in sperm incubated in capacitating media showed a shoulder at ~ 110 nm that was not present in noncapacitated sperm. Fig. 8C shows the distribution of cPKA for individual cells that were incubated only in capacitating media, where the effect is much more evident. As already reported, sperm in capacitating conditions consist of two heterogeneous populations (3), half of the cells capacitate and exhibited a distribution shift from 70 to 110 nm,

PKA relocation in sperm capacitation and acrosome reaction

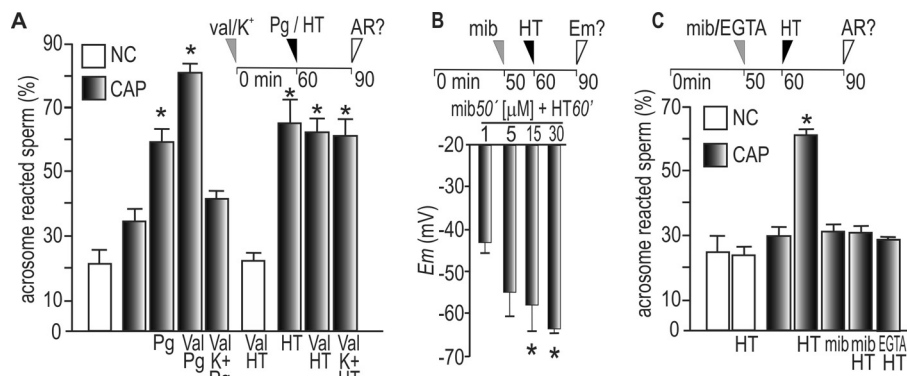


Figure 5. PKA anchoring inhibition induces depolarization of capacitated sperm associated to Ca^{2+} influx. *A*, sperm were incubated for 60 min in noncapacitating (NC, white bars) or capacitating (CAP, gray bars) conditions in the presence or absence of either 1 μM valinomycin (Val) or 1 μM valinomycin + 70 mM KCl (Val K^+) (osmolality was kept constant as in controls). Alternatively, stimulation of the acrosome reaction was performed at 60 min with either 40 μM progesterone (Pg) or 1 μM sHT31 (HT), and acrosomal status (AR) was evaluated after 30 additional min. Data represent mean \pm S.E., $n \geq 3$; *, $p < 0.01$. *B*, sperm were incubated in capacitating conditions during 50 min followed by addition of different mibefradil (mib) concentrations. At 60 min, sperm were challenged with 1 μM sHT31 (HT) and further incubated for 30 min before *Em* analysis. Data represent mean \pm S.E., $n \geq 3$; *, $p < 0.01$. *C*, sperm were incubated for 60 min in noncapacitating (NC, white bars) or capacitating (gray bars) conditions before exposure to 1 μM sHT31 (HT). Alternatively, at 50 min, 5 mM EGTA, or 5 μM mibefradil (mib) were added to the media. Acrosomal status (AR) was evaluated at 90 min. Data represent mean \pm S.E., $n \geq 3$; *, $p < 0.01$.

whereas the other half of the cells showed a distribution of cPKA that is not distinguishable from the cells in noncapacitating media. Addition of 1 μM sHT31 to capacitated sperm promoted a retraction of cPKA to its original dense and compact rod-like radial distribution, clearly showing by microscopy for the first time that disruption of PKA–AKAP interaction alters PKA localization. To further confirm sHT31 as a disruptor of PKA–AKAP interaction, PKARII immunoprecipitations from capacitated sperm in the absence or presence of sHT31 were performed. This experiment aimed to analyze whether PKARII pulls down AKAP4, the most abundant AKAP in the principal piece where PKA localizes. As shown in Fig. 8E, the amount of AKAP4 that co-immunoprecipitates with PKARII was reduced in the presence of sHT31 (Fig. 8E), further supporting that sHT31 disrupts PKA–AKAP interaction.

Discussion

For many years, it has been accepted that molecules involved in cAMP signaling (*i.e.* phosphodiesterases and adenylyl cyclases), as well as its effectors and targets are carefully compartmentalized in sperm (2). This compartmentalization helps assure a tight regulation of different sperm processes associated with capacitation. Although some biological effects of capacitation occur in the head (*e.g.* acrosome reaction), others occur in the tail (*e.g.* hyperactivation). Biochemical immunolocalizations, supported by enzymatic assays, have conclusively demonstrated that PKA in mouse sperm is restricted to the flagellum (24). Further subcompartmentalization would be allowed by local cAMP generation within independently regulated microdomains. These cAMP modules could be in turn modulated by AKAPs, which dock not only PKA but also enzymes and substrates to specific cell locations (25). In this study, we demonstrated that when PKA–AKAP interaction was disrupted by addition of sHT31 before incubation in capacitating conditions, both HCO_3^- (that stimulates ADCY10) and permeable cAMP analogues failed to trigger capacitation, due to impaired *in vivo* PKA activity, as analyzed by Western blotting. This result indicates that PKA needs proper localization to start capacitation events.

Surprisingly, disruption of active PKA from AKAP triggered the acrosome reaction, but *only* in capacitated sperm. On the contrary, noncapacitated sperm did not undergo exocytosis, indicating that disruption of PKA–AKAP interaction can only induce acrosome reaction in cells that have gained fertilizing capacity, associating this phenomenon to a particular physiological state of the cells, rather than to an off-target effect. In addition, the inactive analogue sHT31p did not induce any changes in either capacitated or noncapacitated sperm, further supporting the use of this tool to study specific AKAP disruption effects. The acrosome reaction, triggered by the blockade of PKA–AKAP interaction, involved influx of extracellular Ca^{2+} that started in the principal piece followed by propagation to the mid-piece and the head. Our data substantiate the role of CatSper channels in this Ca^{2+} influx as follows: 1) Ca^{2+} influx started in the principal piece, where CatSper localizes (26), excluding initiation through Cav3.2 or Cav2.3 channels, which localize in the head (27) where Cav2.3 plays a role in the acrosomal reaction (28); 2) pharmacological inhibition of CatSper abolished both Ca^{2+} influx and sHT31-induced acrosome reaction; 3) sperm from CatSper KO mice did not undergo acrosome reaction when challenged with sHT31, but exhibited normal acrosome reaction upon Ca^{2+} ionophore stimulation. This work represents the first report showing that a Ca^{2+} influx through CatSper is conclusively linked to the acrosome reaction. Strikingly, we found that activation of CatSper was promoted by delocalized PKA activity, because blocking the kinase before impairing PKA–AKAP interaction abolished both the acrosome reaction and Ca^{2+} influx. The potential contribution of other proteins to the effects seen upon addition of sHT31 cannot be ruled out, because R2D2 domains, which bind AKAPs, are also found in ROPN1, ASP, SP17, and CABYR (29). However, the fact that the induction of the acrosome reaction by sHT31 was completely blocked by a PKA-specific inhibitor (sPKI) as well as by KT5720, shows that this kinase is a key player in the induction mechanism. Thus, it is compelling to think that this could strike as a novel mechanism for *in vivo* acrosome reaction induction, where sperm cells are exposed to

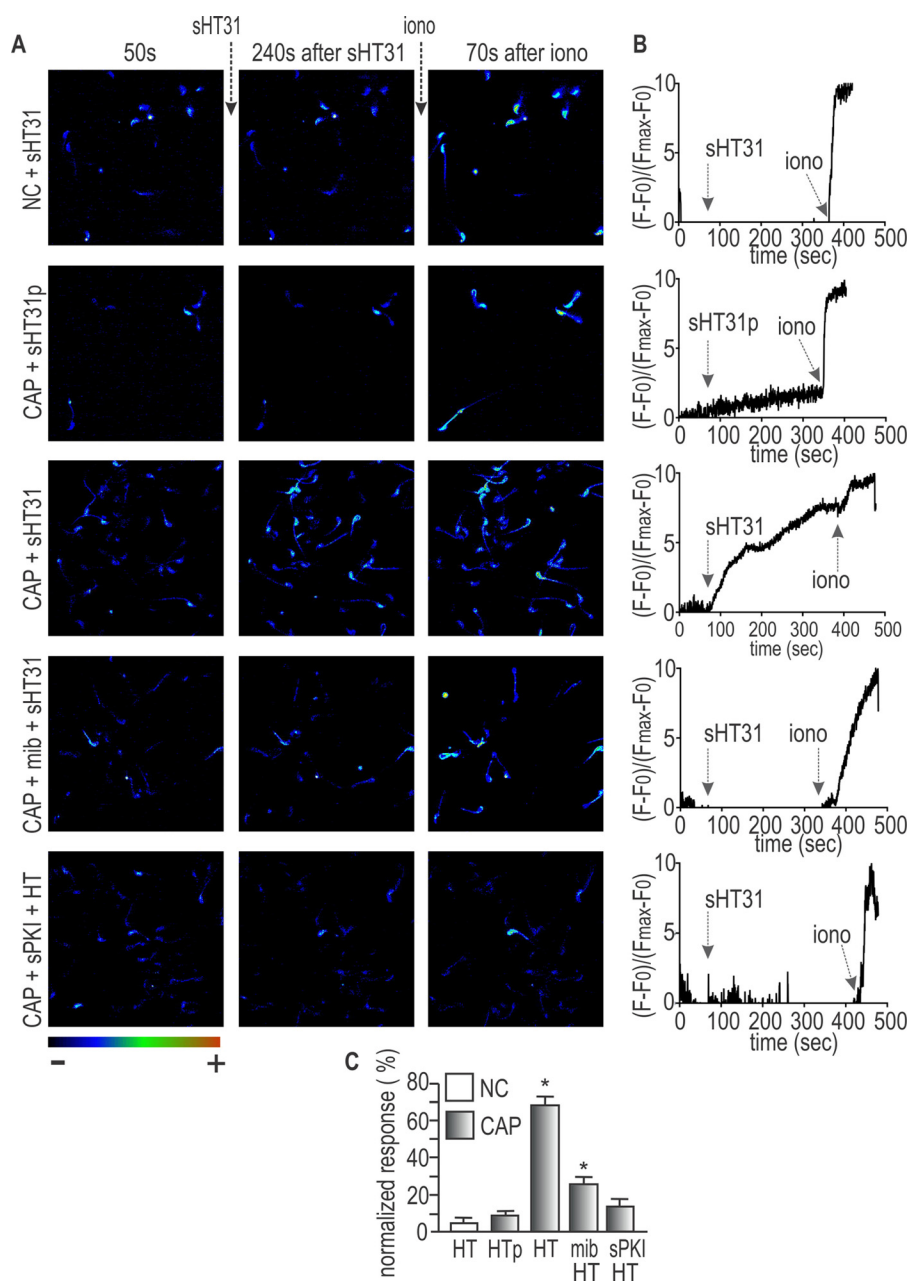


Figure 6. Disruption of PKA–AKAP interaction opens mibefradil-sensitive Ca^{2+} channels. Noncapacitated (NC) and capacitated (CAP) sperm loaded with Fluo3-AM were imaged on laminin-coated coverslips. Fluorescence recordings were captured for 8–10 min at 3 Hz. Alternatively, the cells were preincubated with 5 μM mibefradil (*mib*) or 15 μM sPKI for 10 min before starting the recording. *A*, representative fluorescence images of 5 independent experiments, corresponding to $[Ca^{2+}]_i$ responses obtained before and after sHT31 or sHT31p. At the end 10 μM ionomycin (*iono*) was added as a viability and response control. The color scale from red to blue is shown, where red represents the highest and blue the lowest intracellular Ca^{2+} concentrations. *B*, traces showing representative single cell $[Ca^{2+}]_i$ recordings obtained during each experiment. Arrows indicate additions of sHT31 or sHT31p and ionomycin (*iono*). *C*, percentage of $[Ca^{2+}]_i$ increase induced by sHT31 or sHT31p under the indicated conditions with respect to the increase induced by ionomycin (100%). Data represent mean \pm S.E., $n = 3$, *, $p < 0.01$. See Movies S1–S5 for recordings corresponding to these treatments.

hormones (such as progesterone) and prostaglandins, which could trigger PKA re-localization.

Mice sperm are endowed with the sperm-specific catalytic PKA subunit $Ca2$ (30), lacking myristoylated PKA catalytic subunit $Ca1$ (31), which targets to the plasma membrane. Absence of this isoform abolishes canonical PKA signaling events on the membrane. Then, it is possible that anchoring of PKA to different AKAPs restricts the activity of $Ca2$ to specific locations. Using 3D STORM we show that in noncapacitated sperm, inactive cPKA localizes to a narrow compact rod along the

flagellum with a mean radius of 70 nm. However, after capacitation, cPKA acquired a mean radius of 105 nm. Upon disruption of the PKA–AKAP interaction with sHT31 in capacitated sperm, the cPKA subunit returned to its original location, indicating that PKA anchoring to AKAP is required for re-localization of the enzyme throughout capacitation. This represents the first clear evidence that PKA localization changes during this process.

The regulation of CatSper by PKA awaits further work but opens the possibility to new regulation points of CatSper during

PKA relocation in sperm capacitation and acrosome reaction

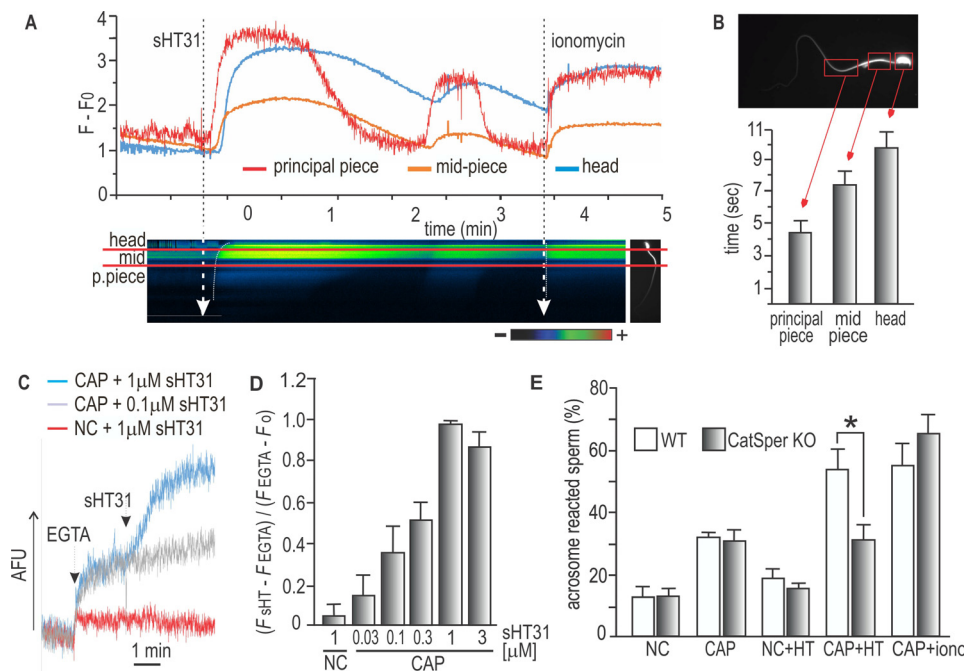


Figure 7. CatSper is involved in the sHT31-induced acrosome reaction. *A*, kymograph of one representative cell of $[Ca^{2+}]_i$ in the different cellular domains, performed using concanavalin A-coated coverslips and increased frame rates (10 Hz, 100 ms/frame), allowing detailed analysis of $[Ca^{2+}]_i$ in sperm subregions (see Movie S6). *B*, bar graph indicates delay times for $[Ca^{2+}]_i$ increase in principal, mid-piece, and head of multiple cell analysis. *C* and *D*, effect of Ca^{2+} removal and subsequent addition of sHT31 on capacitated (CAP) or noncapacitated (NC) sperm loaded with $1 \mu M$ DISC₃(5) during *Em* recordings. *C*, representative recordings are shown for three conditions. *D*, signals are represented as $(F_{sHT} - F_{EGTA}) / (F_{EGTA} - F_0)$, where F_{EGTA} represents fluorescence intensity after 2.5 min EGTA addition, F_0 is the mean of 1 min of acquisition before addition of EGTA, and F_{sHT} represents fluorescence intensity after sHT31 addition. *E*, sperm from either CatSper null mice (CatSper KO, gray bars) or WT siblings (+/-) (WT, white bars) were incubated for 60 min in capacitating (CAP) or noncapacitating (NC) conditions before exposure to $1 \mu M$ sHT31 (HT) or $10 \mu M$ ionophore A23187. Acrosomal status was evaluated at 90 min. Data represent mean \pm S.E.; $n = 4$; *, $p < 0.01$.

sperm capacitation and acrosome reaction. It could be hypothesized that PKA anchoring prevents premature acrosome reaction. However, it could also be possible that *in vivo*, the acrosome reaction is regulated by modification of the PKA-AKAP affinity. To date, apart from the use of high nonphysiological progesterone concentrations, no conclusive physiological inducer of the acrosome reaction has arisen for the mouse model (32). Recent reports have demonstrated that sperm undergo acrosome reaction in the upper segments of the oviduct, prior to contacting the zona pellucida or the progesterone-rich cumulus matrix (33–35). This new pathway where a sudden impairment of the PKA-AKAP interaction triggers the acrosome reaction through CatSper Ca^{2+} influx has the potential to open new courses of research.

Experimental procedures

Chemicals and reagents

Chemicals were obtained from the following sources. BSA (fatty acid-free) and dibutyl-cAMP were purchased from Sigma. sHT31 and sHT31p were from Promega. PKI 14–22 amide and myristoylated (sPKI) were from Tocris. All other chemicals were purchased from Cayman Chemicals (Ann Arbor, MI). α -cPKA (clone 5B) and α -AKAP82 (α -AKAP4) were purchased from BD Biosciences. α -Tyr(P) mAb (α -pY, clone 4G10) was obtained from Upstate Biotechnology (Lake Placid, NY). Rabbit monoclonal α -phospho-PKA substrates (α -pPKAs, clone 100G7E) were purchased from Cell Signaling Technology (Danvers, MA) and α -PKARII from Abcam (num-

ber 38949). Horseradish peroxidase-conjugated α -mouse and α -rabbit IgG, and anti-mouse and α -rabbit IgG light chain (211-032-171 and 115-035-174, respectively) were purchased from Jackson ImmunoResearch Laboratories (West Grove, PA).

Mouse sperm preparation

Cauda epididymal mouse sperm were collected from C57BL/6 young adult male mice (8–13 weeks old) and sacrificed under supervision of the Animal Care and Use Committee of the Facultad de Ciencias Bioquímicas y Farmacéuticas de Rosario (UNR) (protocols approved numbers 7298/532). Each minced cauda epididymis was placed in 500 μ l of a modified Krebs-Ringer solution H-TYH HEPES-buffered medium containing 119.3 mM NaCl, 4.7 mM KCl, 1.2 mM KH_2PO_4 , 1.2 mM $MgSO_4$, 5.6 mM glucose, 0.5 mM sodium pyruvate, 1.7 mM Ca^{2+} , and 20 mM HEPES (pH 7.4). The H-TYH medium accounts for noncapacitating medium. After 20 min, epididymides were removed, and the suspension was adjusted with noncapacitating (NC) medium to a final concentration of $1-2 \times 10^7$ cells/ml. For capacitation (CAP medium), BSA and $NaHCO_3$ were added to final concentrations of 5 mg/ml and 15 mM, respectively. Sperm were then incubated at 37 °C for 60 min. To test the effect of the different inhibitors on capacitation, sperm were preincubated with the respective reagents in noncapacitating medium for 10 min prior to the beginning of the capacitating period.

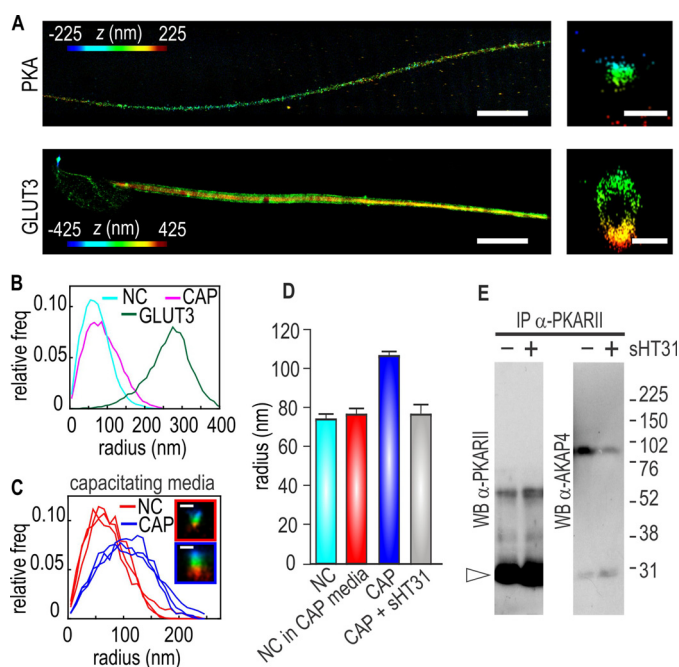


Figure 8. Redistribution of cPKA in mouse sperm during capacitation. *A*, representative color-coded 3D STORM reconstructions of cPKA in the principal piece and GLUT3 in the flagellum and head of capacitated cells. Scale bars: 5 μ m. Right panels show the corresponding Y-Z cross-sections of the 3D STORM reconstructions. Scale bars: 500 nm. *B*, averaged radial distributions of cPKA localization in the principal piece under capacitating (CAP, cyan, $n = 6$) and noncapacitating (NC, pink, $n = 6$) conditions, as well as GLUT3 localization (green). *C*, radial distributions of cPKA in six individual cells under capacitating conditions, where three of them (red) show a distribution similar to noncapacitated (NC) cells and three show a significant shift (blue, CAP). See inserts for Y-Z cross-sections of representative 3D STORM reconstructions, scale bars, 200 nm. *D*, mean radius of cPKA localization in cells incubated in noncapacitating (NC) and capacitating media in the absence (CAP) or presence (CAP + sHT31) of sHT31. Red bar represents mean radius of cPKA of cells that were incubated in capacitating conditions but PKA did not redistribute (red trace of C) (NC in CAP media). *E*, protein extracts from sperm incubated in capacitating conditions in the absence (-) or presence (+) of 3 μ M sHT31 were subjected to immunoprecipitation with α -PKARII antibodies. Immunoprecipitates were analyzed by Western blots with α -PKARII (left panel) and α -AKAP4 (right panel) antibodies. The arrowhead indicates the IgG light chain.

SDS-PAGE and immunoblotting

Sperm were incubated under either noncapacitating or capacitating conditions for 60 min in the presence or absence of different concentrations of sHT31. When the experiment required it, sperm were also incubated with 1 mM Bt₂cAMP + 0.1 mM IBMX or 1 mM 8Br-cAMP + 0.1 mM IBMX (36). After treatment, sperm were twice collected by centrifugation and washed in 1 ml of TBS (150 mM NaCl, 20 mM Tris, pH 7.4). Afterward, cell pellets were re-suspended in Laemmli sample buffer (37) without β -mercaptoethanol, vortexed for 5 s, and boiled for 3 min. After centrifugation, 5% β -mercaptoethanol was added to the supernatants and boiled again for 5 min. Protein extracts equivalent to 1–2 $\times 10^6$ sperm/lane were subjected to SDS-PAGE and electrotransferred to PVDF membranes (Bio-Rad) at 250 mA for 60 min on ice. Membranes were blocked with 3% BSA (Sigma) in TBS containing 0.1% Tween 20 (T-TBS). Antibodies were diluted in T-TBS as follows: α -pY 1/10,000, α -pPKAs 1/3,000, α -PKARII 1/3,000, and α -AKAP4 1/3,000. Secondary antibodies were diluted 1/15,000 in T-TBS and developed using an enhanced chemiluminescence detection kit (ECL Plus, Amersham Biosciences, GE Healthcare)

according to the manufacturer's instructions. When necessary, PVDF membranes were stripped at 60 °C for 15 min in 2% SDS, 0.74% β -mercaptoethanol, and 62.5 mM Tris (pH 6.5) and washed six times for 5 min each time in T-TBS. In all experiments, molecular masses were expressed in kilodaltons (kDa) (38).

PKARII and AKAP4 co-immunoprecipitation

Sperm were capacitated for 90 min. When indicated, 3 μ M sHT31 was added at 60 min, and maintained throughout incubations. Samples were centrifuged at 1,700 $\times g$ for 1 min. The resulting pellet was resuspended in RIPA buffer (10 mM Tris-HCl, pH 7.2, 50 mM NaCl, 0.1% SDS, 1% Triton X-100, 1 mM EDTA, 20 mM sodium fluoride, 40 mM glycerol 3-phosphate and protease inhibitors), incubated on ice for 30 min, and centrifuged at 4 °C for 5 min at 2500 $\times g$. Supernatants containing 1 $\times 10^8$ cells in a final volume of 500 μ l were incubated with 3 μ g of α -PKARII antibody for 2 h at room temperature (23–25 °C) with constant rocking. After the addition of 30 μ l of protein G-Sepharose (GE Healthcare), the reactions were further rocked for 1 h at room temperature. The immune complex was recovered by centrifugation, washed four times in RIPA buffer, and subjected to SDS-PAGE and Western blotting. To avoid immunoreactive signals from IgG heavy chains, rabbit and mouse α -IgG light chain were used.

Mouse eggs collection and in vitro fertilization assays

Female mouse eggs arrested in metaphase II were collected from 6- to 8-week-old super-ovulated CD1 female mice (Charles River Laboratories) at 13 h after human chorionic gonadotrophin (Sigma) intraperitoneal injection. Cumulus cells were removed by brief incubation (<5 min) in H-TYH medium containing 7 mM NaHCO₃, 5 mg/ml of BSA, and 0.02% type IV-S hyaluronidase (Sigma). After cumulus cells removal, eggs were placed in a drop of H-TYH medium containing 22 mM NaHCO₃ and 5 mg/ml of BSA and allowed to recover for 30 min in an incubator with 5% CO₂ at 37 °C. Sperm were capacitated in media containing different concentrations of sHT31 for 60 min, and concentrated by centrifugation at 600 $\times g$ for 3 min. Fertilization drops (200 μ l each) containing 10–20 eggs were inseminated with treated sperm from CD1 male mice (final concentration of 2.5 $\times 10^6$ sperm/ml). Drops contained 0.1 μ M sHT31, which did not affect fertilization. After 4 h of insemination, eggs were washed through brief passages in three drops of H-TYH medium containing 22 mM NaHCO₃ and 15 mg/ml of BSA using a thin bore pipette to detach any loosely attached sperm. After 3 h of further incubation, eggs were fixed with 3.7% paraformaldehyde/PBS for 15 min, washed, and stained with Hoechst 33342 (Sigma, 10 μ g/ml) in PBS for 10 min at room temperature. Fertilization was assessed by visualization of the formation of the male and female pronuclei.

Membrane potential assay in cell populations

After sperm treatment, cells were collected by centrifugation (700 $\times g$, 5 min) and concentration was adjusted to 2.7 $\times 10^6$ sperm/ml. Then, sperm were loaded with 1 μ M of the membrane potential-sensitive dye DISC₃(5) (Molecular Probes) for 5 min. No mitochondrial uncouplers were used because their contribution to the resting potential has been determined to be

PKA relocation in sperm capacitation and acrosome reaction

insignificant (39). The sperm were transferred to a gently stirred cuvette at 37 °C, and the fluorescence was monitored with a Varian Cary Eclipse fluorescence spectrophotometer at 620/670 nm excitation/emission wavelengths. Recordings were initiated when steady-state fluorescence was reached and calibration was performed at the end of each measure by adding 1 μM valinomycin and sequential additions of KCl as previously described (40). Sperm Em was obtained from the initial fluorescence (measured as arbitrary fluorescence units) by linearly interpolating it in the theoretical Em values for the calibration curve against arbitrary fluorescence units of each trace. This internal calibration for each determination compensates for variables that influence the absolute fluorescence values.

For experiments where CatSper opening was assessed, extracellular Ca^{2+} was chelated using EGTA allowing sodium influx through CatSper to occur. The magnitude of the depolarization caused by Na^+ influx relates to the extent of channel opening. Cells were loaded with DISC₃(5) and fluorescence was recorded as detailed above. Calcium was chelated with 3.5 mM EGTA to a value of free calcium of 138 nM (MaxChelator) (17) followed by sHT31 addition. The fluorescence change after and before addition of sHT31 was presented as $(F_{\text{max}} - F)/(F - F_0)$, where F represents fluorescence intensity after EGTA addition, F_0 is the mean of 1 min of acquisition before addition of EGTA, and F_{max} represents fluorescence intensity after sHT31 addition (20, 21).

Stochastic optical reconstruction microscopy (3D STORM)

After sperm incubation in the appropriate condition (NC, CAP, or CAP plus sHT31), they were washed twice with NC media by centrifugation at $2 \times 2,000$ rpm for 5 min and finally resuspended in NC media. Sperm were seeded in poly-L-lysine-coated coverslips (Corning number 1.5), air-dried for 10 min, fixed with 4% (v/v) fresh paraformaldehyde in PBS for 10 min at room temperature, and followed by 3×5 -min PBS washes. Cells were then permeabilized with 0.5% (v/v) Triton X-100 in PBS for 5 min at room temperature and washed 3×5 min with PBS. Samples were blocked with 3% (w/v) BSA/PBS for 1 h at room temperature and then incubated with α -cPKA antibody (1:200) or anti-GLUT3 antibody (1:100) diluted in 1% (w/v) BSA/PBS, overnight at 4 °C in a humidifier chamber. Cells were washed with PBS containing 0.1% (v/v) Tween 20 (T-PBS) at 3×5 min, and further incubated with Alexa Fluor 647-conjugated anti-mouse (1/500) or rabbit (1/1,000) secondary antibody diluted in 1% BSA/PBS for 1 h at room temperature. Cells were then washed with T-PBS twice and PBS once for 5 min each, and immediately mounted in STORM imaging buffer (50 mM Tris-HCl, pH 8, 10 mM NaCl, 0.56 mg/ml of glucose oxidase, 34 $\mu\text{g}/\text{ml}$ of catalase, 10% (w/v) glucose, and 1% (v/v) β -mercaptoethanol). Images were acquired using Andor IQ 2.3 software in a custom-built microscope equipped with an Olympus PlanApo $\times 100$ NA1.45 objective and a CRISP ASI autofocus system (41, 42). Alexa Fluor 647 was excited with a 638-nm laser (DL638-050, CrystaLaser, Reno, NV) under continuous illumination. Initially the photoswitching rate was sufficient to provide a substantial fluorophore density. However, as fluorophores were irreversibly photobleached, a 405-nm laser was introduced to enhance photoswitching. The intensity of the 405-nm laser was adjusted in the range 0.01–0.5 milliwatts to

maintain an appropriate density of active fluorophores. Axial localization was achieved via astigmatism using a MicAO 3DSR adaptive optics system (Imagine Optic, Orsay, France) inserted into the emission pathway between the microscope and the EMCCD camera (43, 44). This technology achieves 3D localization via shaping the axial point spread function, allowing both the correction of spherical aberrations and the introduction of astigmatism. User-controlled introduction of astigmatism enabled the accurate detection of single-molecules over a thickness of 1 μm and, in turn, 3D reconstruction (45). A calibration curve for axial localization was generated with 100-nm Tetra-Speck microspheres (Invitrogen) immobilized on a coverslip (46). The images were acquired in a water-cooled, back-illuminated EMCCD camera (Andor iXon DU-888) operated at -85 °C at a rate of 23 frames/s. 50,000 frames were collected to generate a super resolution image. Single-molecule localization, drift correction using image cross-correlation and reconstruction were performed with Thunder STORM (47).

To find the molecular radial distributions, we selected regions of interest of the flagellum that were found to lie in a straight line. The center of the flagellar cross-section was first found by Gaussian fitting of the localization histograms along x and y . The coordinates of the localized molecules were then transformed into cylindrical coordinates to obtain the radial position r .

Cell-free assay of PKA substrate phosphorylation

Sperm cells (5×10^6 in 60 μl of final volume) were incubated in the presence of different inhibitors (3 μM sHT31 or 15 μM sPKI) for 30 min at 37 °C in H-TYH medium supplemented with: 1% Triton X-100, 40 μM ATP, 1 mM Bt_2cAMP , 0.1 mM IBMX, Sigma protease inhibitor mixture, 100 μM sodium orthovanadate, 5 mM p -nitrophenyl phosphate, 40 mM β -glycerophosphate, and 10 mM MgCl_2 . The presence of Triton X-100 in the assay buffer is responsible for the cell lysis, rendering a “cell-free” assay, and differentiates the experiment from the regular incubation procedure (13). Samples were further subjected to SDS-PAGE and Western blotting followed by immunodetection with an anti-pPKA substrates antibody (clone 100G7E), as described above.

PKA in vitro activity by radioactive assay

Sperm in H-TYH medium were centrifuged at $10,000 \times g$ for 3 min and re-suspended in buffer containing 25 mM Tris-HCl, 150 mM NaCl, protease inhibitor mixture (Roche Applied Science) and 1% Triton X-100 (pH 7.4). Suspensions were incubated on ice for 30 min and then centrifuged at $10,000 \times g$ for 10 min at 4 °C. The supernatant was discarded, and the pellet (Triton insoluble fraction) was re-suspended in 330 μl of the same buffer. This Triton-insoluble fractions were used as source of PKA and its activity was measured as the amount of radioactive phosphate (γ - ^{32}P) incorporated into “Kemptide” (Sigma), which is a specific and synthetic PKA-substrate. The assay mixture was either supplemented or not with inhibitors as described under “Results,” while maintaining constant DMSO concentration ($\leq 0.5\%$).

Sperm motility analysis

Sperm suspensions were loaded on a 20 μM chamber slide (Leja Slide, Spectrum Technologies) and placed on a micro-

scope stage at 37 °C. Sperm movements were examined using the CEROS computer-assisted semen analysis (CASA) system (Hamilton Thorne Research, Beverly, MA). Parameters used were as follows: 30 frames acquired, frame rate of 60 Hz, minimum cell size of 4 pixels, low average path velocity cutoff of 5 mm/s, static head size of 0.2–2.99, static head intensity of 0.26–1.31, and static head elongation lower than 100. At least 20 microscopy fields corresponding to a minimum of 200 sperm were analyzed in each experiment. Hyperactivated sperm were classified according to CASAnova (48).

Acrosomal status assays

After the appropriate treatment, sperm were seeded on 8-well glass slides and air-dried for 15 min. Then, sperm cells were fixed with 3.7% paraformaldehyde in phosphate-buffered saline (PBS, 137 mM NaCl, 10 mM phosphate, 2.7 mM KCl, pH 7.4) for 15 min at room temperature, washed with PBS (four times of 5 min each time), and permeabilized with 0.5% Triton X-100 for 5 min. After washing with PBS, cells were treated with 10% BSA in PBS for 1 h at room temperature and then incubated with Alexa Fluor 488-conjugated peanut agglutinin (1/500) in PBS containing 1% BSA for an extra hour at room temperature. Before mounting with Slow-Fade Light reagents (Molecular Probes), samples were washed with PBS (four times for 5 min each time). Epifluorescence microscopy was performed using a BH2 Olympus microscope. Differential interference contrast images were taken in parallel and they served as the control for sperm morphology.

The acrosomal status was also evaluated by flow cytometry using sperm from transgenic male mice (BDF1-Tg (CAG-mtDsRed2, Acr-EGFP) RBGS0020sb), displaying acrosomal vesicles expressing green GFP fluorescence and mid-pieces (mitochondria) expressing red Ds-Red2 fluorescence (49). Sperm were analyzed on a flow cytometer (FACSCanto II flow cytometer, BD Bioscience) after adding propidium iodide to the sperm suspension to discriminate dead cells. A 515–545-nm band path filter and 650-nm long path filter were used for GFP and propidium iodide, respectively.

Live imaging of intracellular Ca^{2+} levels

After capacitation, sperm were incubated with 2 μ M Fluo3-AM (Molecular Probes) in 0.05% Pluronic acid for 30 min at 37 °C in the dark (15). Then, sperm were washed once at 700 \times g for 5 min and re-suspended in capacitating medium. Once loaded, sperm were immobilized on mouse laminin (0.1 mg/ml)-coated coverslips to allow recordings. The chamber was filled with recording medium (noncapacitating H-TYH) in the absence or presence of 15 μ M sPKI or 5 μ M mibefradil.

All recordings were made at 37 °C and Ca^{2+} imaging was performed before, during, and after addition of recording medium with or without sHT31/sHT31p. Ionomycin (10 μ M) was added at the end of each experiment as a control for cell viability/response, and for posterior normalization. A Zeiss LSM880 scan head on an axio observer Z1 inverted microscope with a \times 60 1.4 NA oil immersion objective was used. Excitation was performed at 488 nm using an argon ion laser, combined with a GaAsP spectral detector with 508–588 nm bandwidth. Bidirectional scanning was used with a dwell time of 1.03 μ s at

512 \times 512 pixels resulting in an acquisition of 2–3 frames/s for periods of 8–10 min. Movies were processed and analyzed in ImageJ (version 1.38, NIH). Regions of interest (ROIs) were drawn on each sperm for fluorescence quantification. The Fluo3 [Ca^{2+}]_i changes are presented as $(F - F_0)/(F_{max} - F_0) \times 10$, where F represents fluorescence intensity at time t , and F_0 is the mean of 1 min of acquisition before any addition. Response to sHT31 or sHT31p for each sperm was normalized against its own ionomycin response (100% response). Mean response of all cells in the experiment was used to compare responses between experiments, and n values represent the number of experiments. Cells with peak [Ca^{2+}]_i changes of >15% relative to the ionomycin changes were counted as responsive. At least 40 cells were analyzed each time, using 3 male mice.

For determination of calcium kinetics, sperm were loaded with Fluo3-AM as described above. Afterward, they were attached to concanavalin A (1 mg/ml)-coated coverslips (instead of laminin) to adhere sperm cells through their head and tail (14). Fluorescence signals were registered with an Eclipse TE300 Nikon inverted microscope using a LED-based pulsed light excitation system and an oil immersion \times 60 objective (PlanApo N, numerical aperture 1.42). Recordings were captured with Andor Ixon-DU8970 EMCCD camera, controlled by iQ software (Andor Technology, Belfast, UK), at 10 images/s with a 2-ms pulse excitation using a single color Cyan LED. To select the desired excitation/emission wavelength we used a bandpass excitation (HQ 485/25X) filter, dichroic mirror (Q-505 LP), and emission (HQ 510 LP) filters (Chroma Technology, Bellows Falls, VT). Image acquisition was done at 10 frames/s for periods no longer than 5 min. Steady initial fluorescence was recorded for 30 s, then 1 μ M sHT31 was added to the recording chamber and fluorescence was registered for 3–4 min more. Ionomycin (10 μ M) was added at the end of the recordings as a control of cell response. Using ImageJ software, we determined separate ROIs for sperm head, mid-piece, and principal piece. Fluorescence from each ROI was background-corrected and normalized using $\Delta F = ((F - F_0)/F_0) \times 100\%$, where ΔF is the percentage change in intensity. For each trace, we then determined the time when fluorescence started to rise and estimated the delay in time-response for each part of the sperm.

Statistical analysis

Paired Student's t test was used to compare mean values between control and tested groups. The difference between mean values of multiple groups was analyzed by one-way analysis of variance followed by Holm-Šidák test. Statistical significances are indicated in the figure legends. At least 100 sperm were analyzed in each case, unless specified.

Author contributions—C. S., C. R., X. X., M. G. G., G. M. L., C. B. G., and Dario Krapf data curation; C. S., C. R., X. X., M. G. G., G. M. L., C. B. G., A. D., Diego Krapf, M. G. B., and Dario Krapf formal analysis; C. S., C. R., X. X., M. G. G., G. M. L., C. B. G., Diego Krapf, M. G. B., P. V., and Dario Krapf investigation; C. S., C. R., X. X., M. G. G., G. M. L., J. L. V.-B., N. I. T., A. D., Diego Krapf, M. G. B., P. V., and Dario Krapf methodology; C. S., C. R., Diego Krapf, P. V., and Dario Krapf writing-review and editing; C. R., P. V., and Dario Krapf conceptualization; Dario Krapf supervision; Dario Krapf funding acquisition; Dario Krapf writing-original draft.

Acknowledgment—We thank Rodrigo Vena for assistance with the LSM880 Zeiss microscope.

References

- Stival, C., Puga Molina Ldel, C., Paudel, B., Buffone, M. G., Visconti, P. E., and Krapf, D. (2016) Sperm capacitation and acrosome reaction in mammalian sperm. *Adv. Anat. Embryol. Cell Biol.* **220**, 93–106 [CrossRef Medline](#)
- Buffone, M. G., Wertheimer, E. V., Visconti, P. E., and Krapf, D. (2014) Central role of soluble adenylyl cyclase and cAMP in sperm physiology. *Biochim. Biophys. Acta* **1842**, 2610–2620 [CrossRef Medline](#)
- Escoffier, J., Navarrete, F., Haddad, D., Santi, C. M., Darszon, A., and Visconti, P. E. (2015) Flow cytometry analysis reveals that only a subpopulation of mouse sperm undergoes hyperpolarization during capacitation. *Biol. Reprod.* **95**, 121 [Medline](#)
- Hernández-González, E. O., Sosnik, J., Edwards, J., Acevedo, J. J., Mendoza-Lujambio, I., López-González, I., Demarco, I., Wertheimer, E., Darszon, A., and Visconti, P. E. (2006) Sodium and epithelial sodium channels participate in the regulation of the capacitation-associated hyperpolarization in mouse sperm. *J. Biol. Chem.* **281**, 5623–5633 [CrossRef Medline](#)
- Stival, C., La Spina, F. A., Baró Graf, C., Arcelay, E., Arranz, S. E., Ferreira, J. J., Le Grand, S., Dzikunu, V. A., Santi, C. M., Visconti, P. E., Buffone, M. G., and Krapf, D. (2015) Src kinase is the connecting player between protein kinase A (PKA) activation and hyperpolarization through SLO3 potassium channel regulation in mouse sperm. *J. Biol. Chem.* **290**, 18855–18864 [CrossRef Medline](#)
- Torres-Quesada, O., Mayrhofer, J. E., and Stefan, E. (2017) The many faces of compartmentalized PKA signalosomes. *Cell. Signal.* **37**, 1–11 [CrossRef Medline](#)
- Li, X., Wang, X., and Snyder, M. (2013) Systematic investigation of protein-small molecule interactions. *IUBMB Life* **65**, 2–8 [CrossRef Medline](#)
- Taylor, S. S., Ilouz, R., Zhang, P., and Kornev, A. P. (2012) Assembly of allosteric macromolecular switches: lessons from PKA. *Nat. Rev. Mol. Cell Biol.* **13**, 646–658 [CrossRef Medline](#)
- Carr, D. W., Hausken, Z. E., Fraser, I. D., Stofko-Hahn, R. E., and Scott, J. D. (1992) Association of the type II cAMP-dependent protein kinase with a human thyroid RII-anchoring protein: cloning and characterization of the RII-binding domain. *J. Biol. Chem.* **267**, 13376–13382 [Medline](#)
- Huang, B., Jones, S. A., Brandenburg, B., and Zhuang, X. (2008) Whole-cell 3D STORM reveals interactions between cellular structures with nanometer-scale resolution. *Nat. Methods* **5**, 1047–1052 [CrossRef Medline](#)
- Rust, M. J., Bates, M., and Zhuang, X. (2006) Sub-diffraction-limit imaging by stochastic optical reconstruction microscopy (STORM). *Nat. Methods* **3**, 793–795 [CrossRef Medline](#)
- Wojtal, K. A., de Vries, E., Hoekstra, D., and van Ijzendoorn, S. C. (2006) Efficient trafficking of MDR1/P-glycoprotein to apical canalicular plasma membranes in HepG2 cells requires PKA-RII α anchoring and glucosylceramide. *Mol. Biol. Cell* **17**, 3638–3650 [CrossRef Medline](#)
- Krapf, D., Arcelay, E., Wertheimer, E. V., Sanjay, A., Pilder, S. H., Salicioni, A. M., and Visconti, P. E. (2010) Inhibition of Ser/Thr phosphatases induces capacitation-associated signaling in the presence of Src kinase inhibitors. *J. Biol. Chem.* **285**, 7977–7985 [CrossRef Medline](#)
- Romarowski, A., Sánchez-Cárdenas, C., Ramírez-Gómez, H. V., Puga Molina Ldel, C., Treviño, C. L., Hernández-Cruz, A., Darszon, A., and Buffone, M. G. (2016) A specific transitory increase in intracellular calcium induced by progesterone promotes acrosomal exocytosis in mouse sperm. *Biol. Reprod.* **94**, 63 [Medline](#)
- Krapf, D., O'Brien, E. D., Cabada, M. O., Visconti, P. E., and Arranz, S. E. (2009) Egg water from the amphibian *Bufo arenarum* modulates the ability of homologous sperm to undergo the acrosome reaction in the presence of the vitelline envelope. *Biol. Reprod.* **80**, 311–319 [CrossRef Medline](#)
- De La Vega-Beltran, J. L., Sánchez-Cárdenas, C., Krapf, D., Hernández-González, E. O., Wertheimer, E., Treviño, C. L., Visconti, P. E., and Darszon, A. (2012) Mouse sperm membrane potential hyperpolarization is necessary and sufficient to prepare sperm for the acrosome reaction. *J. Biol. Chem.* **287**, 44384–44393 [CrossRef Medline](#)
- Patton, C., Thompson, S., and Epel, D. (2004) Some precautions in using chelators to buffer metals in biological solutions. *Cell Calcium* **35**, 427–431 [CrossRef Medline](#)
- Ren, D., Navarro, B., Perez, G., Jackson, A. C., Hsu, S., Shi, Q., Tilly, J. L., and Clapham, D. E. (2001) A sperm ion channel required for sperm motility and male fertility. *Nature* **413**, 603–609 [CrossRef Medline](#)
- Strünker, T., Goodwin, N., Brenker, C., Kashikar, N. D., Weyand, I., Seifert, R., and Kaupp, U. B. (2011) The CatSper channel mediates progesterone-induced Ca²⁺ influx in human sperm. *Nature* **471**, 382–386 [CrossRef Medline](#)
- Ernesto, J. I., Weigel Muñoz, M., Battistone, M. A., Vasen, G., Martínez-López, P., Orta, G., Figueiras-Fierro, D., De la Vega-Beltran, J. L., Moreno, I. A., Guidobaldi, H. A., Giojalas, L., Darszon, A., Cohen, D. J., and Cuasnicú, P. S. (2015) CRISP1 as a novel CatSper regulator that modulates sperm motility and orientation during fertilization. *J. Cell Biol.* **210**, 1213–1224 [CrossRef Medline](#)
- Torres-Flores, V., Picazo-Juárez, G., Hernández-Rueda, Y., Darszon, A., and González-Martínez, M. T. (2011) Sodium influx induced by external calcium chelation decreases human sperm motility. *Hum. Reprod.* **26**, 2626–2635 [CrossRef Medline](#)
- Simpson, I. A., Dwyer, D., Malide, D., Moley, K. H., Travis, A., and Vannucci, S. J. (2008) The facilitative glucose transporter GLUT3: 20 years of distinction. *Am. J. Physiol. Endocrinol. Metab.* **295**, E242–E253 [CrossRef Medline](#)
- Chung, J. J., Shim, S. H., Everley, R. A., Gygi, S. P., Zhuang, X., and Clapham, D. E. (2014) Structurally distinct Ca²⁺ signaling domains of sperm flagella orchestrate tyrosine phosphorylation and motility. *Cell* **157**, 808–822 [CrossRef Medline](#)
- Wertheimer, E., Krapf, D., de la Vega-Beltran, J. L., Sánchez-Cárdenas, C., Navarrete, F., Haddad, D., Escoffier, J., Salicioni, A. M., Levin, L. R., Buck, J., Mager, J., Darszon, A., and Visconti, P. E. (2013) Compartmentalization of distinct cAMP signaling pathways in mammalian sperm. *J. Biol. Chem.* **288**, 35307–35320 [CrossRef Medline](#)
- Greenwald, E. C., and Saucerman, J. J. (2011) Bigger, better, faster: principles and models of AKAP anchoring protein signaling. *J. Cardiovasc. Pharmacol.* **58**, 462–469 [CrossRef Medline](#)
- Qi, H., Moran, M. M., Navarro, B., Chong, J. A., Krapivinsky, G., Krapivinsky, L., Kirichok, Y., Ramsey, I. S., Quill, T. A., and Clapham, D. E. (2007) All four CatSper ion channel proteins are required for male fertility and sperm cell hyperactivated motility. *Proc. Natl. Acad. Sci. U.S.A.* **104**, 1219–1223 [CrossRef Medline](#)
- Escoffier, J., Boisseau, S., Serres, C., Chen, C. C., Kim, D., Stamboulian, S., Shin, H. S., Campbell, K. P., De Waard, M., and Arnoult, C. (2007) Expression, localization and functions in acrosome reaction and sperm motility of Ca(V)3.1 and Ca(V)3.2 channels in sperm cells: an evaluation from Ca(V)3.1 and Ca(V)3.2 deficient mice. *J. Cell. Physiol.* **212**, 753–763 [CrossRef Medline](#)
- Cohen, R., Buttke, D. E., Asano, A., Mukai, C., Nelson, J. L., Ren, D., Miller, R. J., Cohen-Kutner, M., Atlas, D., and Travis, A. J. (2014) Lipid modulation of calcium flux through CaV2.3 regulates acrosome exocytosis and fertilization. *Dev. Cell* **28**, 310–321 [CrossRef Medline](#)
- Newell, A. E., Fiedler, S. E., Ruan, J. M., Pan, J., Wang, P. J., Deininger, J., Corless, C. L., and Carr, D. W. (2008) Protein kinase A RII-like (R2D2) proteins exhibit differential localization and AKAP interaction. *Cell Motil. Cytoskeleton* **65**, 539–552 [CrossRef](#)
- Nolan, M. A., Babcock, D. F., Wennemuth, G., Brown, W., Burton, K. A., and McKnight, G. S. (2004) Sperm-specific protein kinase A catalytic subunit $\alpha 2$ orchestrates cAMP signaling for male fertility. *Proc. Natl. Acad. Sci. U.S.A.* **101**, 13483–13488 [CrossRef Medline](#)
- Hereng, T. H., Backe, P. H., Kahmann, J., Scheich, C., Björås, M., Skålhegg, B. S., and Rosendal, K. R. (2012) Structure and function of the human sperm-specific isoform of protein kinase A (PKA) catalytic subunit $\alpha 2$. *J. Struct. Biol.* **178**, 300–310 [CrossRef Medline](#)
- Buffone, M. G., Hirohashi, N., and Gerton, G. L. (2014) Unresolved questions concerning mammalian sperm acrosomal exocytosis. *Biol. Reprod.* **90**, 112 [Medline](#)

33. Hino, T., Muro, Y., Tamura-Nakano, M., Okabe, M., Tateno, H., and Yanagimachi, R. (2016) The behavior and acrosomal status of mouse spermatozoa *in vitro*, and within the oviduct during fertilization after natural mating. *Biol. Reprod.* **95**, 50 [CrossRef](#) [Medline](#)
34. La Spina, F. A., Puga Molina, L. C., Romarowski, A., Vitale, A. M., Falzone, T. L., Krapf, D., Hirohashi, N., and Buffone, M. G. (2016) Mouse sperm begin to undergo acrosomal exocytosis in the upper isthmus of the oviduct. *Dev. Biol.* **411**, 172–182 [CrossRef](#) [Medline](#)
35. Muro, Y., Hasuwa, H., Isotani, A., Miyata, H., Yamagata, K., Ikawa, M., Yanagimachi, R., and Okabe, M. (2016) Behavior of mouse spermatozoa in the female reproductive tract from soon after mating to the beginning of fertilization. *Biol. Reprod.* **94**, 80 [Medline](#)
36. Krapf, D., Visconti, P. E., Arranz, S. E., and Cabada, M. O. (2007) Egg water from the amphibian *Bufo arenarum* induces capacitation-like changes in homologous spermatozoa. *Dev. Biol.* **306**, 516–524 [CrossRef](#) [Medline](#)
37. Laemmli, U. K. (1970) Cleavage of structural proteins during the assembly of the head of bacteriophage T4. *Nature* **227**, 680–685 [CrossRef](#) [Medline](#)
38. Alvau, A., Battistone, M. A., Gervasi, M. G., Navarrete, F. A., Xu, X., Sánchez-Cárdenas, C., De la Vega-Beltran, J. L., Da Ros, V. G., Greer, P. A., Darszon, A., Krapf, D., Salicioni, A. M., Cuasnicu, P. S., and Visconti, P. E. (2016) The tyrosine kinase FER is responsible for the capacitation-associated increase in tyrosine phosphorylation in murine sperm. *Development* **143**, 2325–2333 [CrossRef](#) [Medline](#)
39. Chávez, J. C., de la Vega-Beltran, J. L., Escoffier, J., Visconti, P. E., Treviño, C. L., Darszon, A., Salkoff, L., and Santi, C. M. (2013) Ion permeabilities in mouse sperm reveal an external trigger for SLO3-dependent hyperpolarization. *PLoS One* **8**, e60578 [CrossRef](#) [Medline](#)
40. Demarco, I. A., Espinosa, F., Edwards, J., Sosnik, J., De La Vega-Beltran, J. L., Hockensmith, J. W., Kopf, G. S., Darszon, A., and Visconti, P. E. (2003) Involvement of a Na⁺/HCO₃⁻ cotransporter in mouse sperm capacitation. *J. Biol. Chem.* **278**, 7001–7009 [CrossRef](#) [Medline](#)
41. Weigel, A. V., Simon, B., Tamkun, M. M., and Krapf, D. (2011) Ergodic and nonergodic processes coexist in the plasma membrane as observed by single-molecule tracking. *Proc. Natl. Acad. Sci. U.S.A.* **108**, 6438–6443 [CrossRef](#)
42. Krapf, D., Campagnola, G., Nepal, K., and Peersen, O. B. (2016) Strange kinetics of bulk-mediated diffusion on lipid bilayers. *Phys. Chem. Chem. Phys.* **18**, 12633–12641 [CrossRef](#) [Medline](#)
43. Izeddin, I., El Beheiry, M., Andilla, J., Ciepielewski, D., Darzacq, X., and Dahan, M. (2012) PSF shaping using adaptive optics for three-dimensional single-molecule super-resolution imaging and tracking. *Opt. Express* **20**, 4957–4967 [CrossRef](#) [Medline](#)
44. Clouvel, G., Jasaitis, A., Sillibourne, J., Izeddin, I., El Beheiry, M., Leveq, X., Dahan, M., Bornens, M., and Darzacq, X. (2013) Dual-color 3D PALM/dSTORM imaging of centrosomal proteins using MicAO 3DSR. in *Conference on Single Molecule Spectroscopy and Superresolution Imaging VI*, San Francisco, CA, February 3, 2013 10.1117/12.2001986 [CrossRef](#)
45. Marbouty, M., Le Gall, A., Cattoni, D. I., Cournac, A., Koh, A., Fiche, J.-B., Mozziconacci, J., Murray, H., Koszul, R., and Nollmann, M. (2015) Condensin- and replication-mediated bacterial chromosome folding and origin condensation revealed by Hi-C and super-resolution imaging. *Mol. Cell* **59**, 588–602 [CrossRef](#) [Medline](#)
46. Huang, B., Wang, W., Bates, M., and Zhuang, X. (2008) Three-dimensional super-resolution imaging by stochastic optical reconstruction microscopy. *Science* **319**, 810–813 [CrossRef](#) [Medline](#)
47. Ovesný, M., Křížek, P., Borkovec, J., Svindrych, Z., and Hagen, G. M. (2014) ThunderSTORM: a comprehensive ImageJ plug-in for PALM and STORM data analysis and super-resolution imaging. *Bioinformatics* **30**, 2389–2390 [CrossRef](#) [Medline](#)
48. Goodson, S. G., Zhang, Z., Tsuruta, J. K., Wang, W., and O'Brien, D. A. (2011) Classification of mouse sperm motility patterns using an automated multiclass support vector machines model. *Biol. Reprod.* **84**, 1207–1215 [CrossRef](#) [Medline](#)
49. Hasuwa, H., Muro, Y., Ikawa, M., Kato, N., Tsujimoto, Y., and Okabe, M. (2010) Transgenic mouse sperm that have green acrosome and red mitochondria allow visualization of sperm and their acrosome reaction *in vivo*. *Exp. Anim.* **59**, 105–107 [CrossRef](#)